Vibrational dynamics of amorphous ice

A. I. Kolesnikov and Jichen Li
Department of Physics, UMIST, PO Box 88, Manchester, M60 1QD, United Kingdom

S. F. Parker and R. S. Eccleston
ISIS Facility, Rutherford Appleton Laboratory, Chilton, Didcot, Oxon, OX11 OQX, United Kingdom

C.-K. Loong
IPNS, Argonne National Laboratory, Argonne, Illinois 60439
(Received 16 July 1998)

Using inelastic neutron scattering, we have measured a range of amorphous forms of ice, including high-density and low-density amorphous ices, in the energy transfer region from 2 to 500 meV (16–4033 cm^{-1}). The measured spectra show that the pressure-produced high-density amorphous ice is significantly different from the two low-density amorphous forms of ice (obtained by vapor deposition and by annealing at 120 K of the high-density amorphous ice), as we expected. However, considerable differences were also observed between the vapor deposits and the low-density amorphous ice obtained from annealing the high-density amorphous ice (the latter has a spectrum very similar to ice-Ih and ice-Ic), indicating that the hydrogen bonding in the two systems are markedly different. [S0163-1829(99)05605-2]

I. INTRODUCTION

Since the discovery of the noncrystalline (amorphous) form of ice by Burton and Oliver in the early 1930s,[1] the understanding of the microscopic properties of amorphous solid water has attracted considerable attention for many decades. Comprehensive experimental investigations, including x-ray,[2,3] electron[3,4] and neutron diffraction (ND),[5–12] infrared (IR) absorption and Raman scattering[13–18] were carried out by various research groups worldwide in order to understand the basic structural and dynamical properties of these amorphous forms of ice. The understanding of the mechanism behind the complex formation and stability of the different kinds of amorphous ice is important to the interpretation of a wide range of unusual behavior related to water in aqueous matter, in living organism and in interstellar objects like comets.

Previous studies have found that there are many different forms of amorphous ice. Their structures and densities vary with the formation conditions and the sample preparation procedures. These ices can be categorized into two types, the high-density amorphous (hda) and low-density amorphous (lda) ice. There are mainly two ways to produce the hda-ice. One is by a pressure treatment, which was realized by two different thermobaric processing methods (through different paths in the P-T phase diagram of ice): (i) pressurizing a crystalline hexagonal ice (ice-Ih) to about 12 kbar at temperatures below 120 K results in an amorphous structure[19] with a density of 1.31 g/cm^3. It is believed that the pressure crushes the open-tetragonal structure of ice-Ih and gives rise to the higher density which is otherwise not obtainable in normal circumstances. This form of hda-ice can be recovered as a metastable state after releasing the pressure at low temperatures ($<$120 K, i.e., below the glass transition temperature) and its density at ambient pressure reduces to 1.17 g/cm^3. (ii) The recovered high-pressure phase ice-VIII can also be transformed to hda-ice by slow warming to about 120 K.[20] It is still an open question, as to what degree these pressure produced hda-ices differ from each other, because the hda-ice from ice-VIII has been annealed above the glass transition temperature.[21]

The other way of producing hda-ice is by vapor deposition at low temperatures ($<$30 K) and low vapor pressures (at 10^{-4} bars, yielding a deposition rate less than 100 μm/h).[2,6] The samples made by this method[6] are in the form of thin layers (0.05 μm) and the results may also depend on the substrate materials. It was believed that at low temperatures and vapor pressures, some water molecules do not have sufficient energy to form the tetrahedrally coordinated structure. As a result, the water molecules can enter interstitial positions in the open ice network (similarly to ice-Ih). The oxygen-oxygen distances between these and surrounding molecules lie between the first and the second coordination spheres corresponding to lda-ice or ice-Ih, and hence the density of this deposited ice is higher. A peculiar property of this vapor deposited hda-ice is its unstable structure; it gradually transforms to a ''restrained'' form of amorphous ice at about 77 K (well below the ice glass transition temperature of $\sim$100 K) and then to a lda-ice at 120 K.[6]

The classification of the lda-ice is equally complex. It was frequently reported that there are many different structures among the lda-ice. It may be reasonable to classify them into two categories: vapor deposited lda-ice[3,6,13,14] and lda-ices obtained by other technique dealing with bulk samples. The latter ices could be obtained by (i) thermal treatment of hda-ices described above;[4,5] (ii) hyperquenching of μm-size water droplets;[12,22] (iii) electron or ion-bombardment of crystalline forms at low temperature.[23,24] All of them have a similar density of $\sim$0.94 g/cm^3. The fundamental difference of these two categories of lda-ice is mainly due to the fact, that for the vapor deposited ice, the deposition process produces a structure with high porosity, resulting in large number of

unconnected hydrogen bonds. On the other hand, the local structures of lda-ice obtained by annealing hda-ice or by vitrification of water droplets are very similar to ice-Ih.

Diffraction studies show that there are some similarities between the different types of hda-ice, e.g., all of them have the first diffraction peak at higher Q values: 2.15 $Å^{-1}$ for the pressure-produced hda-ice[5] and ~1.9 $Å^{-1}$ for vapor deposited ice.[2,6] However, the corresponding Q values for the lda-ice obtained by heating hda-ice and for lda hyperquenched water[9] are 1.70 and 1.79 $Å^{-1}$, respectively.

The most obvious and direct way of examining the observed structure of the amorphous ices is by using x-ray, electron, and ND techniques. The use of x rays for the structural investigation of liquids and amorphous substances is well established and has a long history. However, because of the small charge, hydrogen atoms are almost invisible to x rays (and electrons), but they can be detected by neutrons. Development of the ND technique is relatively recent and has rapidly advanced in condensed matter research in the last twenty years. One of the promising ways is obtaining the partial atom-atom structure factors for amorphous ice by combining the different diffraction techniques and/or by using H_2O/D_2O mixtures in ND (H and D atoms have different amplitudes of coherent neutron scattering). Hence, more complete information on the partial correlation functions can be derived. However, these experiments are difficult due to the fact that H atoms have very large incoherent neutron scattering cross section and the data analysis also requires rather sophisticated corrections for inelasticity effect. For this reason, the results are often not consistent, e.g., various conclusions were given from different research groups concerning the structure of liquid water.[25–27]

The physical properties of ice and water depend on the interactions between the water molecules. Development of a suitable pairwise interaction potential for water is essential to understand the origin of the microscopic behavior of water/ice, including the geometrical conformations of the amorphous ice. After decades of simulations based on a variety of computational techniques, such as molecular dynamics, many effective pairwise potentials were developed, such as TIP4P (Ref. 28) and SK.[29] Their success is still limited to accounting for a few features, such as partial structure factors[27] and density maximum[30] for water. However, none of them are capable of reproducing the vibrational spectra of ice measured by neutron spectroscopy.[31,32] These spectra are directly proportional to the vibrational density of states which can be rigorously calculated by molecular or lattice dynamics calculations using a suitable potential. Thus reproducing the structural properties is not sufficient for the validation of the potentials. Further quantitative comparison of the simulations with the measured vibrational spectra of water/ice is a good criterion in determining the interatomic potentials. This is because the frequencies of the vibrational modes depend on interatomic forces, which are determined by the double derivatives of the pairwise potentials (i.e., $-d^2V/dr^2$), thus the vibrational frequencies are very sensitive to the curvature of the pairwise potential and hence it provides a stringent test of the suitability of the potential. In order to get further progress in the description of the water-water potential, the need for precise experimental data of the vibrational dynamics of different forms of ice is as strong as ever.

II. INELASTIC INCOHERENT NEUTRON SCATTERING TECHNIQUE

Inelastic scattering of thermal neutrons is a unique technique to study vibrational dynamics of molecular substances. First, the energies of the thermal neutrons are comparable to energies of vibrational modes (1–500 meV), the neutron wavelength is of the same order as the interatomic distances in condensed materials and the neutron mass is of the same order as the mass of vibrating atoms, and therefore, the scattering process is very sensitive to the space-dynamical characteristics of the system. Secondly, inelastic incoherent neutron scattering (IINS) spectrum is directly proportional to the vibrational density of states weighted by the atomic mean-square displacements associated with each vibrational mode and by the neutron scattering cross sections of the constituent atoms. Hence, IINS measures all vibrational modes simultaneously and the spectrum provides direct information about intermolecular and intramolecular interactions.

The quantity measured by neutron scattering can be described by the neutron scattering cross section per unit solid angle $d\Omega$ and per unit energy dE:[33]

$$\frac{d^2\sigma}{d\Omega dE} = \frac{k}{k_0} S(\mathbf{Q},E) = \frac{k}{k_0} \sum_{ij} \int_{-\infty}^{\infty} \langle b_i b_j^* e^{i[\mathbf{Q}(\mathbf{r}_i(0)-\mathbf{r}_j(t))]} \rangle e^{iEt/\hbar} dt, \quad (1)$$

where $S(\mathbf{Q},E)$ is a dynamical structure factor, $\mathbf{Q}$ and E are the neutron momentum and energy transfers, k and k_0 are neutron momenta after and before scattering, b_i neutron scattering amplitude for atom i, $\mathbf{r}_i(t)$ the vector position of atom i at time t, the summation is going over all atoms and $\langle ... \rangle$ means averaging over the assemble. The incoherent neutron scattering cross-section for hydrogen atom, $\sigma_H^{\text{inc}} = 4\pi(\overline{b_H^2} - \overline{b_H}^2)$, is much larger (by factor of 10 or more) than for other atoms. On this reason for hydrogen containing materials the dynamical structure factor in Eq. (1) can be transformed to the following expression for IINS contributions $S_{l,k-l}(Q,E)$, due to annihilation of l and creation of $(k-l)$ excitations,

$$S(Q,E) = \sum_{l,k} S_{l,k-l}(Q,E) = \sum_{l,k} \frac{\sigma_H^{\text{inc}}}{4\pi} \exp[-2W(Q)] \times \left(\frac{\hbar^2 Q^2}{2m}\right)^k \int d\omega_1 \ldots d\omega_k \frac{G(\omega_1)\ldots G(\omega_k)}{\omega_1 \ldots \omega_k (k-l)!\, l!} \times \prod_{i=l+1}^{k} [n(\omega_i)+1] \prod_{j=1}^{l} n(\omega_j) \times \delta\left(E - \sum_{i=l+1,k} \hbar\omega_i + \sum_{j=1,l} \hbar\omega_j\right). \quad (2)$$

Here $n(\omega)$ is the population Bose factor, m is a neutron mass, $W(Q)$ is a Debye-Waller factor for hydrogen atom

$$W(Q)=\frac{1}{2}\langle(\mathbf{Qu})^2\rangle=\frac{\hbar}{12m}\int\frac{Q^2G(\omega)}{\omega}[2n(\omega)+1]d\omega. \tag{3}$$

The $G(\omega)$ function introduced in Eqs. (2) and (3) is a generalized vibrational density of states for hydrogen atom, which can be described by a following summation over all normal modes

$$G(\omega)=\sum_j\frac{1}{3M}|\mathbf{e}^j|^2\delta(\omega-\omega_j), \tag{4}$$

where $\mathbf{e}^j$ is the polarization vector of normal modes and M is hydrogen atomic mass.

Equation (2) can be applied to estimate the multiphonon neutron scattering (MPNS) contributions by using the measured data and an iterative technique.[34–36] At the first iterative step, $G(\omega)$ and $W(Q)$ could be calculated from the experimental data based on an assumption that the IINS spectrum of ice is the one-phonon spectrum. At the second and subsequent steps, the difference between the experimental spectrum and that resulting from the multiphonon processes could be accepted as the new one-phonon spectrum. For ice spectra the convergence usually can be reached in few iterations.[36]

Thus the one-phonon part of dynamical structure factor $S(Q,E)$ for IINS spectrum

$$S(Q,E)=\frac{\sigma_H^{\mathrm{inc}}}{4\pi}\exp[-2W(Q)]\frac{\hbar Q^2G(\omega)}{2m\omega}\times[n(\omega)\delta(E+\hbar\omega)+(n(\omega)+1)\delta(E-\hbar\omega)] \tag{5}$$

is directly related to generalized vibrational density of states $G(\omega)$.

This is a clear contrast to Raman and IR spectroscopies, which are insensitive to intermolecular translational and librational modes for ice crystals, because the dipole moments and polarizability induced by these modes, are small. Knowledge of this part of the vibrational spectrum of ice is important in the understanding the nature of hydrogen bonding in the system. For instance, neutron scattering observes two strong peaks at 28 meV (226 cm^{-1}) and 37 meV (298 cm^{-1}),[31,32] while IR and Raman see only one peak at 28 meV. A weak shoulder at 36 meV in the Raman spectrum has been considered to be a combination mode or an overtone.[37] This observation has attracted considerable scientific attention, and renewed efforts in computer simulations have been directed to describe these features in the measured IINS spectra.

In the past few years, we have made a systematic investigation of the phonon dynamics of many exotic crystalline forms of ice using neutron spectroscopy[21,31,32,38–45] and shown that the IINS spectra of ice are very sensitive to their structural changes. In this paper, we present a series of IINS measurements for different amorphous ices: the pressure-produced hda-ice, the lda-ice obtained by annealing of hda-ice and the vapor deposited amorphous ice. The measurements cover a wide range of neutron energy transfers, from 2 to 500 meV, which includes the intermolecular translational and librational vibrations, as well as the intramolecular bending and stretching modes of the water molecule.

III. EXPERIMENTAL

In order to produce a vapor deposited ice, a special center stick for a liquid helium ''orange'' cryostat (OC) has been constructed. The samples were prepared by condensing water vapour (double distilled H_2O or 99.9% purity D_2O) on the surface of an aluminium sample can (hollow cylinder, 60 mm long and 10 mm inner diameter), which was kept at a temperature below 15 K. The temperature of water vapour at the entrance to the sample can was kept at 288 K, in order to prevent blockage of the tip of the vapor jet by ice. The flow rates were monitored by a mass flow controller. To reduce the thermal exchange between the vapor and the substrate surface, low deposition rates (low vapour pressures) were used. The deposition processes were carried out for 45 and 120 h with a flow-rate of 7 and 13 mg/h for H_2O sample (for IINS measurements at TFXA and HET spectrometers,[46] respectively), and 110 h at 20 mg/h for D_2O sample. The estimated sample thicknesses were 0.15 and 0.7 mm for H_2O, and 1.0 mm for D_2O, which corresponded to the rates of samples growth of 3, 6, and 9 μm/h, respectively, and were similar to those used by other groups.[6] After preparation in the cryostat the entire assembly (sample plus cryostat) was installed on the neutron spectrometer. After ND and IINS measurements the samples of the as-prepared vapor deposited ice were transformed to some intermediate states and finally to ice-Ih by heating the sample to several high temperatures (for more details, see the next section).

The hda-ice samples, including H_2O, D_2O and their mixture $(D_2O)_{0.9}(H_2O)_{0.1}$, were prepared by pressuring ice-Ih at 77 K to about 15 kbar. The samples were recovered when the pressure was subsequently released at liquid nitrogen temperature. While submerged in liquid nitrogen, each sample was transferred into an aluminium container, which was attached to the cryostat center stick. The center stick was quickly inserted into closed cycle refrigerator (CCR) or OC precooled at <100 K. The sample volume was evacuated to $\sim$20 mbar and then the sample was cooled to 5 or 15 K, in OC or CCR, respectively. After IINS measurements the H_2O hda-ice was transformed into lda-ice by heating the sample to 120 K at 1 K/min. The structure of the samples was measured by ND. No difference was observed between the IINS spectra for lda-ice and ice-Ih samples, indicating that the configuration and intermolecular interactions of the water molecules in these ice forms, to high accuracy, are the same.

The IINS spectra of prepared ices were measured on different spectrometers, TFXA, HET,[46] and HERMECS (Ref. 47) in order to cover the energy transfer range of 2–500 meV. The TFXA spectrometer (with a fixed scattering angle of $\sim$135° and a fixed final energy $\sim$4 meV) at the ISIS pulsed neutron source (Chilton, UK) was used to obtain high quality data in the energy transfer region from 2 to 150 meV. The use of time and energy focusing, in conjunction with a pyrolytic graphite analyzer in an inverse geometry, allows us to make IINS measurements with very high energy resolution of $\Delta E/E\approx 1\%$. The IINS spectrum of ice measured on TFXA gives poorer information at energy transfers above 150 meV, because at these energies the Debye-Waller factor

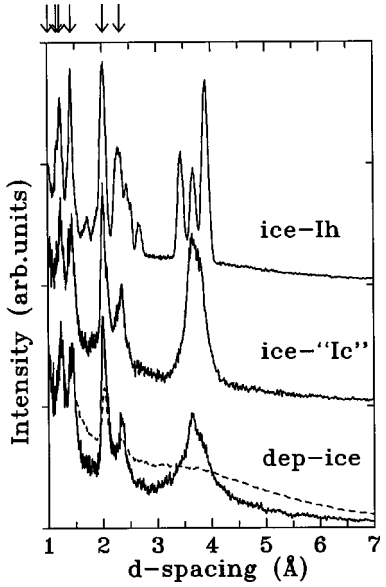

FIG. 1. Powder ND patterns measured on HET at 5 K of the as-prepared deposited ice D_2O (solid curve) and H_2O (dashed curve), and after annealing of the deposited ice D_2O to 185 K (ice-''Ic'') and to 255 K (ice-Ih). The diffraction patterns also contain peaks from the aluminium sample can which are indicated by arrows at top.

significantly suppresses the intensity of the one-phonon part of the spectrum (due to large value of the neutron momentum transfer Q). HET at ISIS or HERMECS at IPNS (Argonne, IL), were used to record high quality spectra at higher energy transfer (up to 600 meV). Both HET and HERMECS are direct-geometry time-of-flight spectrometers; the energy of incident neutrons, E_i, can be selected by a rotating chopper. Hence the measurements of IINS spectra can be made with the incident neutrons having energy very close to the energy region of interest. With correctly chosen conditions (E_i and scattering angle) the neutron momentum transfers at high-energy transfers are much smaller than on TFXA. This made it possible to measure good quality INS spectra for different ice-phases up to the highest phonon energies, around 400–450 meV.[13] In addition, the HET (after removing the neutron chopper) and TFXA spectrometers can perform ND measurements. This flexibility allowed us to measure the structure and vibrational spectra of many prepared ices using the same spectrometers without having to load and reload the samples.

The IINS measurements in most cases were carried out at temperatures at or below 15 K in CCR and OC. The purpose of using the low temperature is to minimize the multiphonon neutron scattering and the temperature effects. The IINS data were transformed to the dynamical structure factor $S(Q,E)$ vs energy transfer using the standard programs for the spectrometers. The background spectra for the empty can in CCR and OC were measured under the same conditions and subtracted from the original data.

IV. NEUTRON DIFFRACTION OF THE VAPOR DEPOSITED ICE

Figure 1 shows the ND patterns measured at 5 K for the vapor deposited H_2O and D_2O samples (see also Ref. 44) in the as-prepared state (dep-ice), as well as for the deposited D_2O sample after its annealing to 185 K (cubiclike ice-''Ic'') and to 255 K (ice-Ih). Because of the large incoherent cross section and the small coherent cross section from H_2O ice ($\sigma_H^{\rm inc}=80.26$ b, $\sigma_H^{\rm coh}=1.7568$ b, $\sigma_O^{\rm inc}=0.0008$ b, and $\sigma_O^{\rm coh}=4.232$ b, $1\,{\rm b}=1\times10^{-24}\,{\rm cm}^2$) in comparison with D_2O ($\sigma_D^{\rm inc}=2.05$ b and $\sigma_D^{\rm coh}=5.592$ b), the scattered intensity for H_2O is dominated by the large, isotropic incoherent neutron scattering background from hydrogen atoms. All the data represent the superposition of structure factors from the ice samples and polycrystalline aluminium (the material of the sample-can, maximum d-spacing for aluminium is 2.34 Å). The position of the right-most peaks for dep-ice D_2O sample has $d=3.7$ Å, which corresponds to the first peak in the structure factor, $S(Q)$, at neutron momentum transfer $Q_1=1.70\pm0.04\,{\rm Å}^{-1}$. This value is in a good agreement with the values for the position of the first peak in the structure factor for lda-ice in the literature.[2–5,7–10,12,19,20]

The first peak in the $S(Q)$ spectrum for amorphous substances with tetrahedrally coordinated molecules is identified as a ''first sharp diffraction peak'' (FSDP) and the origin of this peak can be ascribed to the ordering of interstitial voids around the oxygen atoms comprising the tetrahedrally coordinated continuous-random network structure.[48] The position of the FSDP is given by the simple relation: $Q_1=3\pi/2d$, where d is the average nearest-neighbor atom-void separation (which is equivalent to the average oxygen-oxygen nearest neighbor distance in the case of ice). Thus the d value, or estimated oxygen-oxygen separation in the dep-ice, is 2.77 ±0.10 Å.

Annealing to 185 and 255 K results in the transformation of deposited lda-ice to ice-''Ic'' and ice-Ih; that is seen from the diffraction patterns in Fig. 1. The correlation length, ξ, obtained from the expression $\xi=2\pi/\Delta Q$, where ΔQ, is the full width at half maximum of the first peak in the structure factor, is 26 Å for the D_2O sample, and it is about 11 Å for H_2O dep-ice. The corresponding values for the annealed D_2O samples are 36 and 105 Å for ice-''Ic'' and ice-Ih, respectively. The ξ values for deposited ices are typical for amorphous samples.[2] However, the correlation length for ice-''Ic'', $\xi=36$ Å, is much smaller than for normal crystalline material, and we designated this intermediate quasicubic-like state, as ice-''Ic.'' This state could correspond to the so-called restrained amorphous ice-I_ar, which was observed in Ref. 6 in the sequence of transformations during annealing of vapor deposited hda-ice (called as I_ah) to lda-ice (at temperatures between 40 and 70 K, called as I_al) and to I_ar (at $T=144$ K).

We did not observe the hda-ice from ND measurements; all the vapor deposits were the lda-ice as observed by other ND experiments.[3,7] The plausible reason for this may be that in the neutron scattering experiments bulk samples were used (mass of ~1 g and thickness of ~1 mm), while in transmission electron microscope measurements[6] the hda-ice I_ah was in the form of thin layers (~0.05 μm thick), and thus it represents only the surface features. The formation of I_ah during vapor deposition can be due to the specific bonding preference of water molecules on the surface.[49,50]

V. INTERMOLECULAR VIBRATIONS FOR HDA AND LDA ICE

All known ices (except for ice-X, which has an ioniclike structure) are molecular substances, which consist of well-

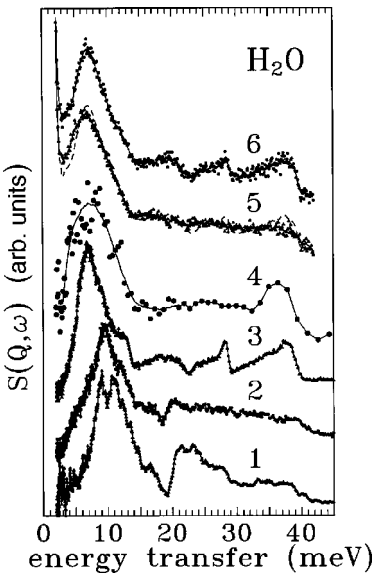

FIG. 2. The IINS spectra (H_2O) in the range of intermolecular translational vibrations measured at $T=5$ K on TFXA for ice-VI (curve 1), hda-ice (curve 2), ice-Ih (curve 3), and dep-ice (Ref. 51) (curve 4), and on HET ($E_I=45$ meV) for dep-ice (curve 5) and after annealing to 215 K, ice-Ih (curve 6). For clarity the plotted spectra are shifted along the y axis. The solid curves are the polynomial-smoothed data. The dashed line plotted over curve 5 is the smoothed spectrum of the ice-Ih for better visual comparison.

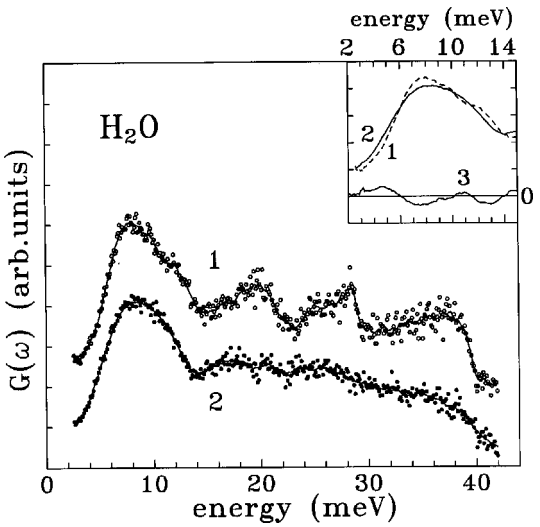

FIG. 3. The generalized vibrational density of states (translational bands) transformed from the $S(Q,\omega)$ spectra (Fig. 2, curves 5 and 6) for the as-prepared deposited ice H_2O (full circles, curve 2) and after annealing to 215 K, ice-Ih (open circles, curve 1). The curves are the polynomial-smoothed data. The inset shows these curves and their difference (curve 3) in the energy transfer region below 15 meV.

separated water molecules interacting with each other via hydrogen bonds. The forces between atoms in the water molecule are much stronger than the hydrogen bond forces (the parameters corresponding to intramolecular O-H stretching force and O-H...O hydrogen bond used in LD calculations[31,32] were 36.1 and 2.1 eV/Å^2, respectively). Hence the vibrational spectra of ice can be subdivided into intermolecular vibrations at less than 120 meV and intramolecular vibrations between 200 and 450 meV without overlap. The intermolecular part could be further subdivided into two bands due to translational ($<$40 meV) and librational (50–120 meV) vibrations of water molecules. The intramolecular vibrations could be assigned to bending, ν_2, at about 200 meV and stretching modes, ν_1 and ν_3, at about 420 meV, according to the internal degrees of freedom within a water molecule.

Figure 2 shows the IINS spectra of two amorphous ice forms, the hda-ice and dep-ice. The spectra of crystalline phases ice-Ih and ice-VI (Refs. 40 and 41) are also shown in the figure for comparison. The spectra were measured on the TFXA (curves 1 to 4) and HET (curves 5 and 6) spectrometers. The ice-Ih sample measured on HET (curve 6) was obtained by heating the dep-ice to 215 K in the OC on the HET spectrometer. Thus the measurements for dep-ice and ice-Ih were carried out under exactly the same conditions (the temperature for both samples during the measurements was 5 K). At energy transfers less than 6 meV, there is a pronounced extra intensity in the IINS spectrum for the as-prepared deposited ice when compared to ice-Ih. Figure 3 shows the translational band of the generalized vibrational density of states $G(\omega)$ for these two ice forms, obtained from the measured $S(Q,\omega)$ spectra.

The inset in Fig. 3 shows the $G(\omega)$ for dep-ice and ice-Ih at energy transfers below 15 meV. The difference spectrum (curve 3) clearly reveals the excess of vibrational states in addition to acoustic phonons in the region 3 to 6 meV in the deposited amorphous ice. This is the so called low energy excitation (LEE) or ''boson'' peak,[51] which is commonly observed in the vibrational spectra of amorphous substances. This result is in agreement with earlier work,[52] which showed the existence of the localized low frequency modes in simulated deposited amorphous ice. The origin of this peak may be associated with the distortion of the local structure due to the topological disorder in amorphous substances, and it is believed that this peak is responsible for the excess of specific heat in the region between 1 and 20 K. By normalizing the translational part of the spectra to three (which is the three degrees of freedom per water molecule) the integrated intensity under the difference curve of $G(\omega)$ in the range of LEE (2–6 meV), or the number of LEE per water molecule, is found to be 0.028 (or about 0.01 LEE/atom). The value for deposited glassy propylene ($CH_2=CHCH_3$) and 1-butene ($CH_2=CHCH_2CH_3$) is equal to 1.64 and 1.4 LEE/molecule[53] (or 0.18 and 0.12 LEE/atom), respectively, and 0.02 and 0.007 LEE/atom for typical tetrahedrally-coordinated glasses SiO_2 and Se, respectively.[54]

The librational bands for the H_2O samples and the translational and librational bands for the D_2O samples for the amorphous forms and crystalline phases[40,41] are shown in the Figs. 4 and 5, respectively. In the translational part of the IINS spectra (see Fig. 2) for the as-prepared vapor deposited ice H_2O and after annealing to 215 K (ice-Ih), the position of the first peak is observed at about the same energy value, $\sim$7 meV. This value is in good agreement with the energy of the acoustic peak in the low-density forms of ice, Ih, Ic, and lda-ice in the literature.[31,32,40–42,45] This indicates that their bulk densities are very close to each other. This peak shifts to higher energy for the high-pressure forms of ice (Figs. 2 and 5). Its position for hda-ice is at 9.6 meV for H_2O and at

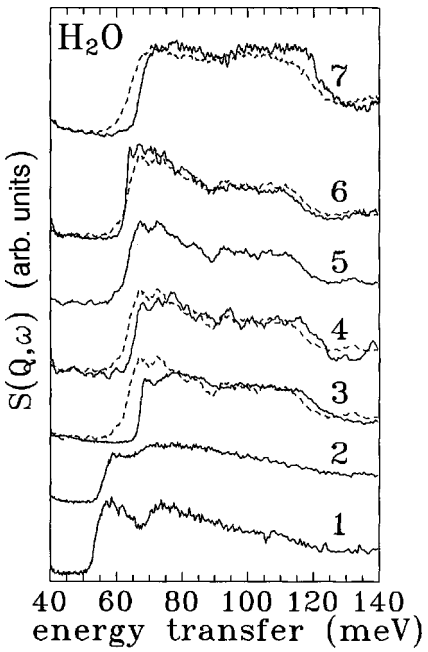

FIG. 4. The IINS spectra (H_2O) in the range of intermolecular librational vibrations measured at $T=5$ K on TFXA for ice-VI (curve 1), hda-ice (curve 2), ice-Ih (curve 3), dep-ice (Ref. 51) (curve 5), after annealing dep-ice to 185 K (curve 4) and ice-IX (Ref. 46) (curve 6), and on HET ($E_I=170$ meV) for the dep-ice (dashed curve 7) and after annealing of dep-ice to 215 K, ice-Ih (solid curve 7). The curves are the polynomial-smoothed data. The dashed curves over the solid curves 3, 4, and 6 are the spectrum for dep-ice, curve 5, plotted for visual comparison.

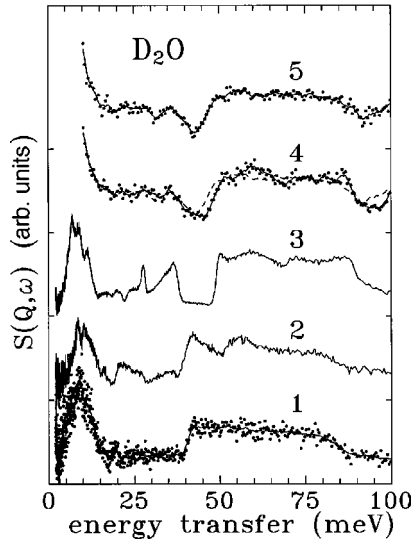

FIG. 5. The IINS spectra (D_2O) measured at $T=5$ K on TFXA for hda-ice (curve 1), ice-VI (curve 2), and ice-Ih (curve 3), and on HET ($E_I=130$ meV) for the dep-ice (Ref. 51) (curve 5) and after annealing of dep-ice to 215 K, ice-Ih (curve 4). The curves are the polynomial-smoothed data. The dashed curve over the solid curve 4 is the spectrum for dep-ice (curve 5) plotted for visual comparison.

~9 meV for D_2O samples, and the peak splits for ice-VI with maxima at 9.0 and 11.0 meV for H_2O and 8.5 and 10.5 meV for D_2O.

It follows from the above data, that there is no long-range order in the deposited ice, because the correlation length obtained from ND is very short ($\xi=11$ Å) and the translational part of the IINS spectrum above 15 meV is featureless (i.e., does not exhibit any peaks), but its structure is relaxed (the number of LEE/atom is much less compared to other deposited amorphous materials, such as propylene and 1-butene). On the other hand the lda-ice, produced by heating the hda-ice, has shown[32] that its IINS spectrum was very similar to those for low-density crystalline phases, ice-Ih and ice-Ic. That means, the lda-ice may have extended-range or at least medium-range order.

The librational part of the IINS spectra for H_2O hda-ice, dep-ice and intermediate state ice-''Ic'' and ice-Ih, obtained by heating dep-ice to 185 and 230 K, respectively, are shown in Fig. 4, together with ice-VI and IX for comparison purposes. It was found that the characteristic value for the librational band in the IINS spectrum for different ice forms is the position of its low-energy cut-off. As shown in Fig. 4, the low-energy cut-off of the librational band for the as-prepared deposited ice (curve 5) is shifted by about 3.5 meV to lower energy compared to ice-Ih (curve 3). This shift is even higher for hda-ice (curve 2) and ice-VI (curve 1), about 11 and 13 meV, respectively. Assuming the moment of inertia for water molecules in these ices is about the same, the result indicates that the transverse forces between the water molecules are smaller for the higher density ices. The latter suggests also that the oxygen-oxygen nearest distances are longer in these ices compared to ice-Ih.

It is seen from the comparison in Fig. 4 that the librational part of the INS spectrum of the dep-ice resembles that of ice-IX (curve 6) in many details, but not the spectrum for normal ice-Ih or other forms of ice. This indicates that the transverse intermolecular force constants between nearest-neighbor water molecules, which mainly determine the behavior of the librational band, are very similar for the vapor deposited ice and ice-IX. The spectrum for the deposited sample annealed at 185 K, quasi-cubic-like ice-''Ic'' (or perhaps relaxed amorphous), is also considerably different from that for ice-Ih. This observation means that the vibrational spectrum of the ice-''Ic'' is definitely different from the spectra for low density ices (Ih, Ic, and lda-ice).[32]

From the above analysis we can conclude, that the characteristic features of the IINS spectrum for hda-ice (the en-

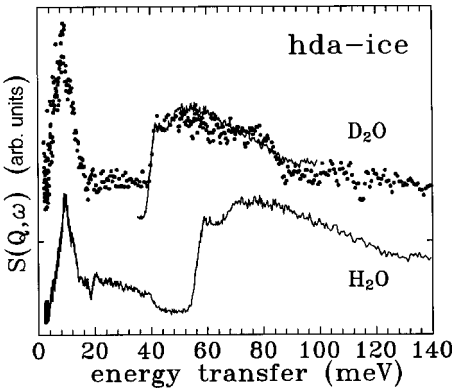

FIG. 6. The IINS spectra measured at $T=5$ K on TFXA for hda-ice H_2O and D_2O (the bottom curve and top points, respectively). The curve plotted above points at the top is the librational band of the IINS spectrum for H_2O with energy scale reduced by factor $\sqrt{2}$ (see the text).

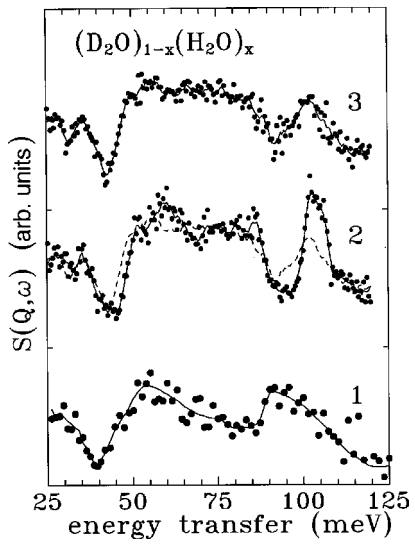

FIG. 7. The IINS spectra of $(D_2O)_{1-x}(H_2O)_x$ measured at $T=5$ K on HERMECS ($E_I=150$ meV) for hda-ice ($x=0.10$, curve 1) and on HET ($E_I=130$ meV) for dep-ice (Ref. 51) ($x=0.05$, curve 3) and ice-Ih (curve 2). The curves are the polynomial-smoothed data. The dashed curve over ice-Ih spectrum (curve 2) is the spectrum of dep-ice plotted for visual comparison.

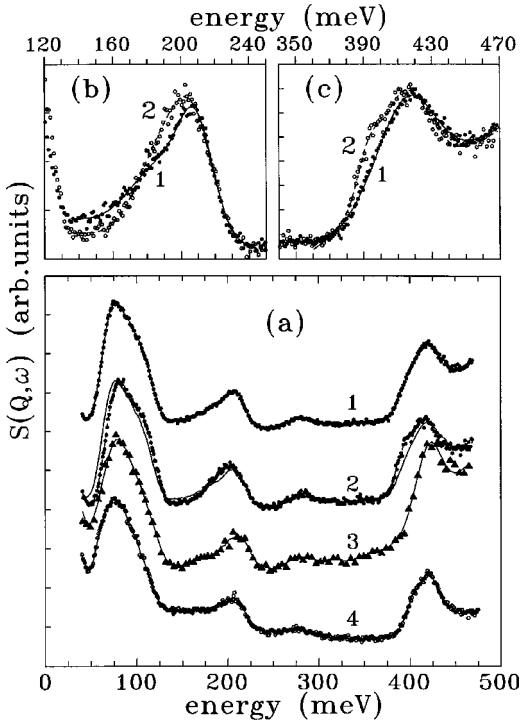

FIG. 8. The IINS spectra (H_2O) measured at $T=5$ K on HET for dep-ice (points and solid curve 1) and ice-Ih (open points and dashed curve 2) with $E_I=500$ meV and for ice-VI (Ref. 47) (open points and curve 4) with $E_I=600$ meV, and on HERMECS ($E_I=500$ meV) for the hda-ice (triangles and curve 3). The curves are the polynomial-smoothed data. The solid curve over the spectrum for ice-Ih is the spectrum of dep-ice plotted for visual comparison. The spectra are shown in the energy transfer range: (a) 0–500 meV (the plotted spectra are shifted along the y axis); (b) 120–250 meV, bending modes (lines are two Gaussian fits); and (c) 340–470 meV, stretching modes (lines are one and two Gaussian fits for as-prepared deposited ice and ice-Ih, respectively). The parameters of the fits are in Table I.

ergy positions of the first ''acoustic'' peak, at about 9 meV, and the low-energy cut-off of the librational band, at 40 and 56 meV, for D_2O and H_2O) are very similar to ice-VI. The differences are: the spectrum for ice-VI shows well defined splitting of the first acoustic peak, two optic peaks in the translational part ($\sim$21 and $\sim$35 meV) and two peaks in the range of the librational band. All these features are missing from the hda-ice spectrum, which looks unstructured in the optic part of the translational band and in the whole area of the librational band. Extra intensity is seen in the acoustic part (below $\sim$8 meV) of the hda-ice spectrum, compared to ice-VI, for both isotopic forms. This extra intensity has a similar origin to that for the deposited amorphous ice discussed above. The peaks at around 20 and 28 meV in ice-Ih are missing in the spectra of the amorphous hda-ice. Absence of long range order in hda-ice structure could be responsible for the broad featureless behavior in this part of the spectra.

Figure 6 shows a comparison of hda-ice spectra for H_2O and D_2O samples. The first peak in both spectra are at the same energy. Surprisingly, the spectra exhibit harmonic isotope behavior for their librational parts. The librational band for H_2O sample, energy scaled by a factor of $\sqrt{I(D_2O)/I(H_2O)} \approx \sqrt{2}$, where I is the moment of inertia, well describes the measured spectrum for D_2O hda-ice. This means that the potentials experienced for the two isotopic forms of water in hda-ice are the same (within the detectable error margin) and it very close to harmonic at low temperature.

The librational parts of the spectra for the mixture of D_2O and H_2O hda-ice (curve 1, 10% H_2O in D_2O measured on HERMECS) and dep-ice (curve 3, 5% H_2O in D_2O measured on HET) are shown in Fig. 7. The spectrum for ice-Ih (curve 2, dep-ice heated to 255 K and then measured on HET) are also plotted for comparison.[44] The hydrogen local mode peak in the spectrum of ice-Ih can be fitted with two narrow Gaussians placed at 102.7 and 106.4 meV. The local mode peak in the spectrum of dep-ice is at slightly lower energy, about 102 meV, but has much larger width [full width at half maximum (FWHM) $\approx$10 meV]. The position of the local mode peak for hda-ice is at the lowest energy, around 97 meV, with FWHM of $\sim$16 meV. We can conclude that (i) the transverse forces acting on the water molecules in hda-ice are much weaker than in dep-ice and ice-Ih, and (ii) the distribution of these forces (which is proportional to the FWHM of the local mode peak) in amorphous ices is much greater than in ice-Ih.

VI. INTRAMOLECULAR VIBRATIONS

The IINS spectra of the dep-ice, ice-Ih (produced by heating dep-ice to 255 K), hda-ice and ice-VI in the energy transfer region below 500 meV are shown in Fig. 8. The peaks around 200 and 420 meV are due to the bending and stretching modes, respectively. The stretching mode peaks for the crystalline phases, ice-Ih and ice-VI, are clearly split into two components, while those for the amorphous samples look like single peaks. The positions of the bending and stretching mode peaks determined by fitting to Gaussian functions are listed in Table I. Lines in Figs. 8(b) and 8(c)

show the fitted spectra for dep-ice and ice-Ih, measured at exactly the same conditions. The bending mode peaks for all samples can be fitted with two Gaussians. The positions of the Gaussians for the bending mode peaks of ice-Ih, dep-ice, and ice-VI are about the same, but they are more split for hda-ice. For the stretching mode peaks, an increase of the energy positions is observed in the following sequence: ice-Ih→dep-ice→ice-VI→hda-ice. This indicates that the O-H covalent-bond distances in the water molecules of the corresponding ice forms are decreasing. Moreover, due to the ordering of the oxygen positions in the ice-Ih and ice-VI and disordering in the amorphous ices, one should expect a sharper splitting of the peaks in the spectrum of the crystalline phases (due to the symmetric and asymmetric stretching modes of water molecules) and a broad peak for the amorphous ices, due to the broader distribution of forces acting to the water molecules. This behavior was observed for the spectra of ice-Ih and ice-VI (splitting of the stretching mode peak) and dep-ice (the peak broadening), but not for the hda-ice. The stretching mode peak for hda-ice is much narrower. This case will be discussed below after consideration of the MPNS processes and time-independent background corrections.

The peak seen at about 285 meV can be explained by MPNS, mainly due to simultaneous excitation of intramolecular bending modes and intermolecular librational modes. The librational-librational two-phonon contributions are expected to be at energy transfers about 180 meV, that is in the region of bending modes. To separate and remove these contributions, which is important at high neutron momentum transfers, we have calculated the MPNS spectrum (up to four-phonon processes) in a harmonic isotropic approximation using the measured data and the iterative technique as described earlier.

Figure 9(a) shows the measured $S(Q,\omega)$ and calculated MPNS spectra for dep-ice and ice-Ih. As we supposed, the peak at about 285 meV is indeed due to the MPNS contributions. The derived one-phonon spectra in the ranges of bending and stretching modes are shown in parts (b) and (c) of Fig. 9. The MPNS contributions in the stretching mode region are smooth and do not influence the peak position of the derived one-phonon spectra [see Fig. 9(c) and Table I]. The effect of the MPNS in the range of the bending modes is very strong. Because the MPNS spectrum arises mainly from the double convolution of the librational band, and the librational band for the deposited ice is about 3.5 meV softer than that for ice-Ih, the calculated MPNS peak for the deposited ice is by about 7 meV softer compared to that for ice-Ih. The shape of the derived one-phonon bending peaks in Fig. 9(b) differs from that of the experimental spectra, it is more symmetrical after the subtraction of the MPNS contribution. Hence we believe that the left hand peak found in the Gaussian fit of the bending mode peaks is an artifact due to the MPNS processes.

The background of IINS spectra measured on the direct-geometry time-of-flight spectrometers at energy transfers close to the energy of the incident neutrons (E_I) increases noticeably. The collected neutron scattering data are proportional to the number of neutrons that arrive at the detectors, and are a function of the time-of-flight from the moderator to the sample position (L_1) and sample position to detector

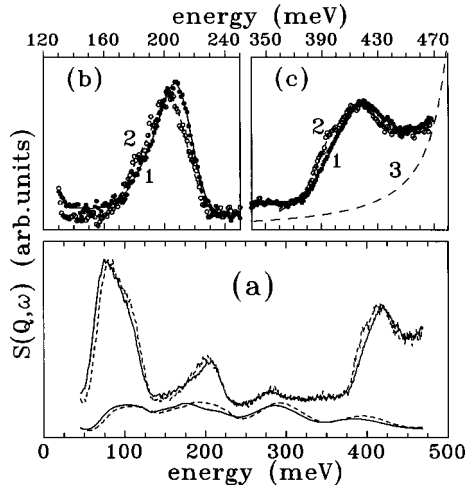

FIG. 9. (a) The IINS spectra (H_2O) measured at $T=5$ K on HET ($E_I=500$ meV) for dep-ice (solid curve) and ice-Ih (dashed curve). The curves are the polynomial-smoothed data from Fig. 8. The bottom curves are the calculated MPNS contribution. The curves in the parts (b) and (c) show the extracted one-phonon spectra for dep-ice (solid points and solid curve 1) and ice-Ih (open points and dashed curve 2) in the range of bending and stretching modes, respectively. The long-dashed curve in part (c) shows an estimated time-independent background [see the text and expression (7)].

(L_2). The time-of-flight spectra, $F(t)$, are usually transformed to representations of neutron energy transfer, $F(E)$ [or $S(Q,E)$, see previous]. The relationship between the time-of-flight, t, and the neutron energy transfer, E, and $F(t)$ and $F(E)$ spectra are

$$t(E)=\frac{L_1}{\alpha\sqrt{E_I}}+\frac{L_2}{\alpha\sqrt{E_I-E}} \tag{6}$$

and

$$F(E)=F(t)\frac{dt}{dE}=F(t)\frac{L_2}{2\alpha(\sqrt{E_I-E})^3}, \tag{7}$$

where α is a coefficient. It is seen from Eq. (7) that, if the measured $F(t)$ spectrum has any small time-independent background, the corresponding $F(E)$ spectrum will have a singularity at $E=E_I$.

We have approximated this background by use of the expression (7) [shown as a long dashed curve in Fig. 9(c)] and subtracted it from the one-phonon spectra. The resulting stretching modes data are shown in Fig. 10 (see also Table I). The average position of the stretching mode peak (obtained by fitting with one Gaussian) is 414.1 meV (FWHM=55 meV) for ice-Ih and 417.5 meV (FWHM=36 meV) for ice-VI. Thus this value for ice-Ih is about 4 meV softer than for the dep-ice and ice-VI. This is about 1.5 times larger than the shift for the stretching mode peaks for the dep-ice and ice-Ih ($22\,cm^{-1}=2.7$ meV), observed in the Raman spectra.[13] The highest shift is 12 meV observed for hda-ice. The shift can be attributed to the difference in oxygen-hydrogen covalent bond length, which is a function of the oxygen-oxygen separation distance. Using an empirical relation between the energy of the stretching mode

TABLE I. The energy positions and full width at half maximum (in brackets) of the fits with Gaussian functions for the IINS spectra of the as-prepard deposited ice (dep-ice), ice-Ih (produced by heating the dep-ice to 255 K), ice-VI and hda-ice. The values are in meV. (*) The time-independent backgound-corrected data (see the text).

	Bending modes				Stretching modes					
	Experimental data		Derived one-phonon data		Experimental data		Derived one-phonon data		Background-corrected data*	
ice-Ih	189.2	208.0	181.7	203.6	392.3	413.1	392.7	413.5	393.5	415.7
	(35)	(27)	(21)	(27)	(14)	(36)	(36)	(36)	(12)	(51)
dep-ice	189.9	209.0	194.1	209.5		414.9		415.7		418.5
	(44)	(23)	(31)	(22)		(39)		(38)		(50)
ice-VI	188.7	208.2			401.2	418.7			401.2	418.7
	(39)	(24)			(12)	(33)			(12)	(33)
hda-ice	185.0	211.8				420.9				426.0
	(50)	(27)				(30)				(51)

and the oxygen-oxygen distances at different pressures in ice,[55] one can find that compared to ice-Ih the O—O distances are 0.03 Å longer in the dep-ice and ice-VI, and ~0.08 Å longer in the hda-ice. Thus the estimated oxygen-oxygen separations are ~2.78 Å in the dep-ice and ice-VI, and ~2.83 Å in the hda-ice. The similar estimates from Raman data for hda-ice made in Ref. 16 was 2.82 Å. The structural x-ray[4] analysis for hda-ice gives a value of 2.8 Å. From the ND study[56] the oxygen-oxygen distances in ice-VI are 2.726 to 2.788 Å (the average is 2.774 Å).

VII. CONCLUSIONS

The measured IINS spectra for the amorphous H_2O and D_2O dep-ice and hda-ice, compared to their crystalline analogues, such as ice-Ih and ice-VI, show that the energy positions of the first peak in the acoustic part of the spectra are about the same, but the data reveal additional low-energy excitations below the first acoustic peak and ''smoothed'' behavior of the high energy part of the translational band. The spectra for dep-ice compared to ice-Ih show softening of the entire librational band by 3.5 meV, and a shift to higher energy for the bending mode peak by 5.9 meV (difference between the main peaks) and for the stretching mode peak by 4.4 meV. The librational bands in the IINS spectra of hda-ice and ice-VI show similar behavior, but the bending and stretching modes peaks for hda-ice are shifted to higher energy compared to ice-VI by about 3.6 and 8.5 meV, respectively. The shifts to lower energy for the librational band and to higher energy for the bending and stretching modes can be explained by the fact that the oxygen-oxygen distances between nearest-neighbor water molecules are longer: (i) in the dep-ice than in other low-density ices, such as ice-Ih, ice-Ic and lda-ice; and (ii) in hda-ice than in ice-VI. The peaks in the IINS spectra at about 285 meV and the left-hand shoulder around 185 meV are of MPNS origin. For this reason the bending mode peaks seen could be described by a single Gaussian only (the higher energy component in Table I).

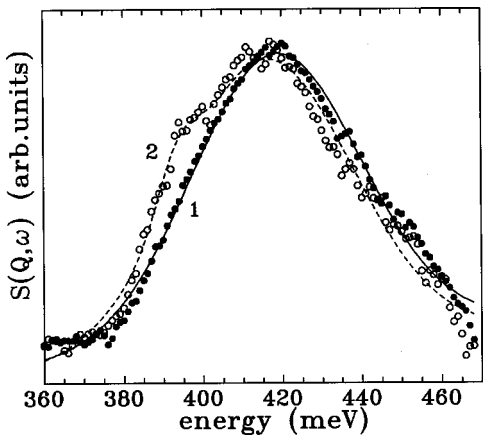

FIG. 10. The stretching mode peaks for H_2O dep-ice (solid points and solid curve 1) and ice-Ih (open points and dashed curve 2) derived from the IINS spectra measured on HET after correction for MPNS and time-independent background.

The data obtained clearly indicate that the low-temperature and low-rate water vapor deposition has produced a low-density amorphous ice, which differs from another low-density amorphous ice, obtained by heating to ~120 K the hda-ice at ambient pressure, and very strongly differs from the hda-ice. The hda-ice, produced by pressurising the ice-Ih at 77 K to 15 kbar, has a lot of similarities with ice-VI, obtained at the same pressure at room temperature and then slowly cooled down to 77 K.

ACKNOWLEDGMENTS

This work was supported by a research grant from the Engineering and Physical Sciences Research Council, and we acknowledge the use of the neutron facility at the Rutherford Appleton Laboratory (UK) and at Argonne National Laboratory (supported by the U.S. DOE-BES under Contract No. W-31-109-ENG-38).

[1] E. F. Burton and W. T. Oliver, Proc. R. Soc. London, Ser. A **153**, 166 (1935).
[2] A. H. Narten, C. G. Venkatesh, and S. A. Rice, J. Chem. Phys. **64**, 1106 (1976).
[3] J. Wenzel, C. U. Linderstrøm-Lang, and S. A. Rice, Science **187**, 428 (1975).
[4] A. Bizid, L. Bosio, A. Defrain, and M. Oumezzine, J. Chem. Phys. **87**, 2225 (1987).
[5] M.-C. Bellissent-Funnel, J. Teixeira, and L. Bosio, J. Chem. Phys. **87**, 2231 (1987).
[6] P. Jenniskens and D. F. Blake, Science **265**, 753 (1994).
[7] M. R. Chowdhury, J. C. Dore, and J. T. Wenzel, J. Non-Cryst. Solids **53**, 247 (1982).
[8] M. C. Bellissent-Funel, L. Bosio, A. Hallbrucker, E. Mayer, and R. Sridi-Dorbez, J. Chem. Phys. **97**, 1282 (1992).
[9] J. C. Dore, J. Mol. Struct. **237**, 221 (1990).
[10] M. C. Bellissent-Funel, J. Teixeira, L. Bosio, J. Dore, and P. Chieux, Europhys. Lett. **2**, 241 (1986).
[11] M. A. Floriano, E. Whalley, E. C. Svensson, and V. F. Sears, Phys. Rev. Lett. **57**, 3062 (1986).
[12] A. Hallbrucker, E. Mayer, L. P. O'Mard, J. C. Dore, and P. Chieux, Phys. Lett. A **159**, 406 (1991).
[13] T. C. Sivakumar, D. Schuh, M. G. Sceats, and S. A. Rice, Chem. Phys. Lett. **48**, 212 (1977).
[14] T. C. Sivakumar, S. A. Rice, and M. G. Sceats, J. Chem. Phys. **69**, 3468 (1978).
[15] M. S. Bergren, D. Schuh, M. G. Sceats, and S. A. Rice, J. Chem. Phys. **69**, 3477 (1978).
[16] D. D. Klug, O. Mishima, and E. Whalley, Physica B **139&140**, 475 (1986).
[17] I. Engquist, I. Lundström, Bo Liedberg, A. N. Parikh, and D. L. Allara, J. Chem. Phys. **106**, 3038 (1997).
[18] A. Givan, A. Loewenschuss, and C. L. Nielsen, J. Phys. Chem. B **101**, 8696 (1997).
[19] O. Mishima, L. D. Calvert, and E. Whalley, Nature (London) **310**, 393 (1984); **314**, 76 (1985).
[20] A. M. Balagurov, O. I. Barkalov, A. I. Kolesnikov, G. M. Mironova, E. G. Ponyatovskii, V. V. Sinitsyn, and V. K. Fedotov, JETP Lett. **53**, 30 (1991).
[21] A. I. Kolesnikov, V. V. Sinitsyn, E. G. Ponyatovsky, I. Natkaniec, L. S. Smirnov, and J.-C. Li, J. Phys. Chem. B **101**, 6082 (1997).
[22] E. Mayer, J. Appl. Phys. **58**, 663 (1985).
[23] H. G. Heide, Ultramicroscopy **14**, 271 (1984).
[24] H. G. Heide and E. Zeitler, Ultramicroscopy **16**, 151 (1985).
[25] W. E. Thiessen and A. H. Narten, J. Chem. Phys. **77**, 2656 (1982).
[26] A. K. Soper and R. N. Silver, Phys. Rev. Lett. **49**, 471 (1982).
[27] J. C. Dore, in *Water Science Reviews*, edited by F. Franks (Cambridge University Press, Cambridge, 1985), Vol. 1, p. 3.
[28] W. L. Jorgensen, J. Chandrasekhar, J. D. Madura, R. W. Impey, and M. L. Klein, J. Chem. Phys. **79**, 926 (1983).
[29] M. Sprik and M. L. Klein, J. Chem. Phys. **89**, 7556 (1988).
[30] C. H. Cho, S. Sing, and G. W. Robinson, J. Chem. Phys. **107**, 7979 (1997).
[31] J-C. Li and D. K. Ross, in *Physics and Chemistry of Ice*, edited by N. Maeno and T. Hondoh (Hokkaido University Press, Sapporo, 1992), p. 27.
[32] J. Li, J. Chem. Phys. **105**, 6733 (1996).
[33] W. Marshall and S. W. Lovesey, *Theory of Thermal Neutron Scattering* (Clarendon Press, Oxford, 1971).
[34] A. I. Kolesnikov and E. F. Sheka, Sov. Phys. Solid State **25**, 1303 (1983).
[35] B. Renker, H. Schober, and F. Gompf, J. Low Temp. Phys. **105**, 843 (1996).
[36] A. I. Kolesnikov and J.-C. Li, Physica B **234–236**, 34 (1997).
[37] P. T. T. Wong, D. D. Klug, and E. Whalley, in *Physics and Chemistry of Ice*, edited by E. Whalley, S. J. Jones, and L. W. Gold (Royal Society of Canada, Ottawa, 1973), pp. 87–92.
[38] A. I. Kolesnikov, J.-C. Li, D. K. Ross, O. I. Barkalov, V. V. Sinitsyn, and E. G. Ponyatovsky, Phys. Lett. A **168**, 308 (1992).
[39] J-C. Li, J. D. Londono, D. K. Ross, J. L. Finney, J. Tomkinson, and W. F. Sherman, J. Chem. Phys. **94**, 6770 (1991).
[40] J-C. Li, J. D. Londono, D. K. Ross, J. L. Finney, S. M. Bennington, and A. D. Tayor, J. Phys.: Condens. Matter **4**, 2109 (1992).
[41] J-C. Li and D. K. Ross, Nature (London) **365**, 327 (1993).
[42] J-C. Li and D. K. Ross, J. Phys.: Condens. Matter **6**, 10 823 (1994).
[43] J-C. Li, D. K. Ross, and M. H. B. Hayes, J. Mol. Struct. **322**, 131 (1994).
[44] A. I. Kolesnikov, J-C. Li, S. Dong, I. F. Bailey, R. S. Eccleston, W. Hahn, and S. F. Parker, Phys. Rev. Lett. **79**, 1869 (1997).
[45] A. I. Kolesnikov, V. V. Sinitzin, E. G. Ponyatovsky, I. Natkaniec, and L. S. Smirnov, J. Phys.: Condens. Matter **6**, 375 (1994).
[46] 1992 ISIS User Guide to Experimental Facilities, SERC, edited by B. Boland and S. Wapham, 75 pp.
[47] IPNS Progress Report 1991–1996, Vol. 1, edited by B. Morzec (Argonne National Laboratory, 1996), 168 pp.
[48] S. R. Elliot, J. Chem. Phys. **103**, 2758 (1995).
[49] V. Bush, J. Chem. Phys. **96**, 3814 (1992).
[50] F. J. Bermejo, A. Criado, and J. L. Martinez, Phys. Lett. A **195**, 236 (1994).
[51] V. K. Malinovsky, V. N. Novikov, P. P. Parshin, A. P. Sokolov, and M. G. Zemlyanov, Europhys. Lett. **11**, 43 (1990).
[52] M. Cho, G. R. Fleming, S. Saito, I. Ohmine, and R. M. Stratt, J. Chem. Phys. **100**, 6672 (1994).
[53] O. Yamamuro, I. Tsukushi, T. Matsuo, K. Takeda, T. Kanay, and K. Kaji, J. Chem. Phys. **106**, 2997 (1997).
[54] M. A. Ramos, L. Gil, A. Bringer, and U. Buchenau, Phys. Status Solidi A **135**, 477 (1993).
[55] D. D. Klug and E. Whalley, J. Chem. Phys. **81**, 1220 (1984).
[56] W. F. Kuhs, J. L. Finney, C. Vettier, and D. V. Bliss, J. Chem. Phys. **81**, 3612 (1984).